INTENSIVE SUBSTORMS DURING THE MAIN PHASE OF THE MAGNETIC STORM ON MARCH 23-24, 2023

© 2025 L. I. Gromova[a, *], N. G. Kleimenova[b, **], S. V. Gromov[a], K. K. Kanonidi[a], V. G. Petrov[a], L. M. Malysheva[b]

[a]*Pushkov Institute of Terrestrial Magnetism, Ionosphere and Radio Wave Propagation RAS, Moscow, Troitsk, Russia*

[b]*Schmidt Institute of Physics of the Earth, RAS, Moscow, Russia*

**e-mail: gromova@izmiran.ru*

***e-mail: ngk1935@yandex.ru*

Received February 29, 2024

Revised June 21, 2024

Accepted July 25, 2024

Abstract. Here we studied the planetary features of the spatiotemporal distribution of ionospheric electrojets recorded in the substorm onset and in the time on the activity maximum of three very intense substorms (with the *AL*-index from -1200 nT to -1700 nT) observed during the main phase of the strong magnetic storm on 23−24 March 2023. We analyze the substorms by applying the global maps of the planetary distribution of the high-latitude ionospheric currents, constructed on the basis of the simultaneous magnetic measurements on 66 low-orbit satellites of the AMPERE project, as well as the ground-based magnetograms from the Scandinavian IMAGE profile and mid-latitude IZMIRAN stations located in the same longitudinal region. It was established that the onset of all the studied substorms at the IMAGE meridian was accompanied by the development of a night-time current vortex with a clockwise rotation direction that is an indicator of the downward field-aligned currents increasing. The ground-based mid-latitude observations at the IZMIRAN station network confirmed that the center of the substorm current wedge was located in the night-time sector significantly east of the IMAGE meridian. In the time of the substorm intensity maximum, a similar but more extensive current vortex was observed in the morning sector, that fact is, probably, typical for intense substorms.

Keywords: *magnetic storm, substorm, ionospheric and field-aligned currents*

DOI: 10.31857/S00167940250610e4

1. INTRODUCTION

The main phase of a magnetic storm is of fundamental importance in the study of energy transfer processes in the solar wind - magnetosphere - ionosphere system. Practically all magnetic storms in their main phase are accompanied by intense substorms, for example [Akasofu and Chapman, 1963], and the stronger the storm, the more intense the substorms [Feldstein et al., 1997], since both these phenomena have a common cause - the southern component of the interplanetary magnetic field (*Bz* MMP < 0).

There are a great number of individual papers and reviews devoted to the study of various aspects of the development of substorms observed both during magnetic storms and in their absence. In early papers, e.g., [Kamide et al., 1982; Hsu and McPherron, 2000], the authors found no difference between these substorms. At the same time, when comparing the distribution of the magnetic field in the tail of the magnetosphere during substorms associated and not associated with magnetic storms, significant differences were found in [Baumjohann et al.,1996], which allowed us to assign them to different types of substorms.

Later in [Hoffman et al., 2010], a study of the peculiarities of the accompanying substorm visible auroral glow on the Polar satellite during 16 moderate and strong magnetic storms was carried out in comparison with similar glow during isolated substorms not associated with magnetic storms. Their significant differences were established, manifested, first of all, in the fact that the substorms during the storms were not accompanied by the development of auroral *bulge* and the development of double oval, i.e., auroral bifurcation (according to the terminology of [Gjerloev et al., 2008]).

However, other researchers did not confirm this conclusion. For example, Kornilova and Kornilov [2009] analyzed data from ground-based television observations of polar auroras in Lovozero Observatory during the main phase of 10 magnetic storms and concluded that "storm" substorms can be accompanied by the development of auroral bulge. Lovozero during the main phase of 10 magnetic storms, they concluded that "storm" substorms can be accompanied by the development of auroral bulge both in the form of a jump-like displacement of auroral arcs toward the pole and in the form of bright diffuse patches of auroras, rapidly spreading in different directions. The characteristics of the auroras depended on many reasons: parameters of the solar wind and the IMF, local magnetic time (MLT), the source that caused this magnetic storm, and others.

Thus, there is still no clear understanding of whether there are fundamental differences between substorms during storms and without them, and, if so, what kind of differences they are. Also, the global peculiarities of the spatial and temporal dynamics of substorm development during substorms of different types and intensities of magnetic storms, even on the examples of analyzing individual events, are clearly insufficiently investigated. The purpose of this paper– is to study intense

magnetospheric substorms during magnetic storm March 23−24, 2023, one of the first strong storms in the 25th solar activity cycle.

2. MAGNETIC STORM March 23−24, 2023

Magnetic storm 23− March 24, 2023 was the first strong (minimum *SymH* value ~ – 170 nTL) storm of solar activity cycle 25. It occurred in the fourth year of the development of the growth phase of the solar cycle, which is the second in the epoch of reduced solar activity [Ishkov, 2023] and was caused by the arrival to the Earth of disturbances from the interaction of coronal mass ejections that occurred during possible flare events on March 20, 2023 (https://www.izmiran.ru/services/saf/archive/). As shown in [Ishkov, 2022], the most powerful (for a given cycle) flare events within epochs usually occur in the decline phase of the cycle and in the initial stage of the minimum phase, more rarely in the growth phase and in the maximum phase, so the appearance of such a strong magnetic storm at the threshold of the solar cycle maximum attracted universal attention.

The main phase of the magnetic storm began around 10 UT on March 23 with the appearance of a stable negative *SymH* gradient. However, its development was rather slow due to the unstable and strongly varying near zero *Bz*-component of the MMP. And only at ~17:30 UT on March 23 with a sharp turn of the IMF to the south, the main phase began to develop actively.

We investigated the interval of the active development of the main phase of the storm (c ~17:40 UT 23 March, when the *Bz* MMP turned southward, to 03 UT 24 March), which was characterized by little changing velocity (440− 490 km/s) and weak dynamic pressure (25 nPa) of the solar wind; at the same time, the magnitude of the *Bz* component of the MMP changed weakly during 9 h, remaining in the range from ~– 11 nTL to ~– 16 nTL (Fig. 1).

Fig. 1.

During this period, several intervals of increasing substorm activity were observed, expressed in a sequence of intense substorms with the AL-index reaching– 1200,– 1500,– 1700 nTL, synchronously with which the *PC*-index, as an indicator of solar wind energy entering the magnetosphere [Troshichev et al., 2014], increased significantly. Fig. 1 shows that the increase of the *PC-index* was the same before the analyzed substorms, which is the result of the practically unchanged solar wind speed and the value of the *Bz*-component of the MMP in the time interval under consideration, and only the change of the sign of the *By*-component from positive to negative and the jump of the solar wind density at 00 UT on March 24 led to the fact that the third substorm developed under slightly different conditions than the first and second ones.

The features of these three substorms will be discussed in more detail below.

3. DATA USED

As an indicator of substorms, we used the graphical representation of the classical *AL*-index (https://wdc.kugi.kyoto-u.ac.jp/wdc) rather than the frequently used 1-min SML-index, which is calculated according to the *AL*-index calculation methodology, but for all stations of the SuperMAG network (https://supermag.jhuapl.edu/indices/) in the magnetic latitude band from 40 to 80°. Note that the *SML*-index data become important in the study of large magnetic storms when the equatorial boundary of the oval and the position of the western electrojet are shifted below the auroral stations used to calculate the *AL*-index.

Unfortunately, to date, the SuperMAG network does not yet have magnetic data from Tiksi (TIK) and Dikson (DIK) stations for the March 23-24, 2023 event, which are very important for the assessment of geomagnetic disturbances in the auroral zone during the time interval under study. However, these data are already available at the Kyoto WDC, and the *AL*-index calculated taking into account them can be considered as the most reliable. However, the numerical values of this index are not yet available at the WDC Kyoto site.

The global distribution of substorms was analyzed using the maps of ionospheric currents presented by the AMPERE (*Active Magnetosphere and Planetary Electrodynamics Response Experiment*) project at the site (http://ampere.jhuapl.edu/products). They are constructed on the basis of simultaneous magnetic measurements of 66 low-orbit (780 km) satellites. The AMPERE maps are presented in the AAGCM coordinate system (MLAT, MLT) with a 1° latitude step and data averaged over a 10-minute interval with a 2-minute offset (https://ampere.jhuapl.edu/info/). We refer each map to the middle of the averaging interval.

The uniform position of satellites over the Earth's surface gives a picture of the planetary distribution of geomagnetic activity, which we cannot obtain from the ground data, since the stations are located unevenly due to large oceanic expanses, and/or due to the lack of observation points (e.g., in Siberia). The uniformity of satellite data coverage of the Earth's surface makes the analysis of AMPERE maps preferable to the analysis of SuperMAGa maps.

The study also used ground data of the meridional profile of the Scandinavian network of IMAGE (*International Monitor for Auroral Geomagnetic Effects*) project magnetometers (https://space.fmi.fi/image/) located at latitudes 57-78° MLAT at approximately the same longitude, MLT = UT+2.7, and midlatitude stations of the IZMIRAN network (partially available at the site (http://serv.izmiran.ru), located in the same longitude sector as the meridional profile of IMAGE stations. IMAGE is currently virtually the only available network of magnetometers among which one can select a chain of stations densely spaced in latitude along a single meridian, almost from the polar cap to− considering data from the IZMIRAN network− low latitudes. The stations belonging to the North American SuperMAG magnetometer network are located at different latitudes and

longitudes, and there is no possibility to select a similar chain of magnetometers forming a sufficiently long latitudinal profile along the same meridian.

Variations of the MMP and solar wind parameters, as well as the *SymH* storm activity index, were investigated using 1-min data from OMNI (https://omniweb.gsfc.nasa.gov/), PC-index− using data from the website (https://pcindex.org).

4. GLOBAL SUBSTORM DYNAMICS DURING THE MAIN PHASE OF A MAGNETIC STORM

We consider the peculiarities of the global development of substorms during the main phase of a magnetic storm using AMPERE maps of the distribution of ionospheric currents at high latitudes (above 60° MLAT) of the Northern Hemisphere of the Earth. In Fig. 2, for each considered substorm, we present maps of the position of ionospheric electrojet currents before the *onset* of the substorm at the time of the substorm *onset* and near its maximum activity (by *AL*-index).

Fig. 2.

Substorm-1, which began approximately one hour after the *Bz* IMF rotation to the south, was preceded by a 3-hour interval in which weak geomagnetic activity was observed, hence, this substorm was an isolated substorm. The AMPERE 18:00- 18:10 UT map (Fig. 2*a*, left map) shows the development of quiescent convective currents prior to the onset of the substorm. At the moment of substorm onset (center map, 18:40-18:50 UT in Fig. 2*a*), we observed the formation of a powerful current vortex in auroral latitudes with clockwise rotation, strengthening of the western electrojet around midnight and its sharp shift to the pole in the evening sector, as well as significant strengthening of the eastern electrojet and its movement to lower latitudes. The map 18:56 - 19:06 UT (Fig. 2*a*, right map), constructed for the moment of the maximum of substorm activity, shows the expected shift of the electrojet to lower latitudes and an increase in its longitudinal size.

Unexpected was the formation of a significant current vortex with clockwise rotation in the morning sector (~05− 08 MLT) at latitudes above ~70° MLAT. The center of the vortex is located above Siberia. At this time in the evening sector (~15− 18 MLT) at lower latitudes, compared to the morning vortex, a less intense vortex with the opposite direction of rotation is observed.

Substorms-2 and *-3*, which followed Substorm-1, were observed near the maximum activity of the main phase of the magnetic storm and were characterized by increasing intensity.

Substorm-2 began to develop immediately after the abrupt end of a small magnetic perturbation separating *substorms-1* and *-2* at the background of geomagnetic activity slightly increased during the main phase of the storm. Before the beginning of the substorm (left map 21:02− 21:12 UT in Fig. *2b*), the ionospheric electrojets were more intense than before substorm-1 and shifted to lower latitudes. The onset of substorm-2 (center map 21:16 - 21:26 UT in Fig. 2*b*) was accompanied by the

development of a current vortex in the early morning sector, but not in the near-midnight sector, where a complex superposition of two vortices with opposite rotation directions was observed at this time, but at lower latitudes than in the case of substorm-1. By the time of the maximum activity of the substorm (right map 21:46 - 21:56 UT in Fig. 2*b*), the electrojets had further intensified, with the westerly one shifting toward the pole and the easterly one toward lower latitudes. As in substorm-1, the formation of an intense current vortex with a clockwise rotation direction was observed in the morning sector (05− 08 MLT), and in the evening sector - a much weaker vortex of the opposite rotation direction, the center of which was located at lower latitudes than in the first substorm.

The development of ***substorm-3*** began at an even more perturbed background than *substorm-2* at the *AL* index value ~ -500 nTL. Ionospheric electrojets before the beginning of *substorm-3* were more intense than before *substorm-2* and shifted to lower latitudes (left map 23:52− 00:02 UT in Fig. *2c*). The beginning of this substorm, as in the previous cases, was associated with the appearance of a current vortex with a clockwise rotation direction in the night sector, but at higher near-pole latitudes (center map 00:00 - 00:10 UT in Fig. *2c*). Note that the development of this vortex occurred after a sharp change in the sign of the *By* MMP from positive to negative and a jump in the dynamic pressure of the solar wind. It is known, for example [Boudourides et al., 2003], that solar wind pressure jumps can shift the polar edge of the auroral oval toward the pole.

5. DEVELOPMENT OF SUBSTORMS AT THE IMAGE MERIDIAN

In the previous section the spatial and temporal dynamics of substorms was considered on a global scale on the basis of maps that represent the instantaneous distribution of ionospheric currents at latitudes above 60° MLAT of the northern hemisphere of the Earth. The temporal dynamics of the development of substorms in a narrow longitude sector can be analyzed from the IMAGE Scandinavian chain magnetograms.

In Fig. 3 presents the magnetograms of the *X*- and *Y*-components of the geomagnetic field of the IMAGE meridional profile stations during the analyzed interval of the main phase of the magnetic storm.

Fig. 3.

Substorm-1 (*AL* up to− 1200 nTL) on the IMAGE profile, which was at this time in the evening sector, began at subauroral latitudes (~61° MLAT, OUJ) and quickly spread to polar latitudes, reaching the maximum activity at 19 UT at latitudes 71− 74° MLAT. According to the sharp spike in the *Y*-component of the magnetic field, *substorm-1* can be attributed to WTS-type substorms (*Westward Traveling Surge*), which is characterized by the fact that the ionospheric current directed along the north-south meridian is generated in the region of increasing electron bursts, where such a spike is observed [Ebihara and Tanaka, 2015; Kisabeth and Rostoker, 1973; Tighe and Rostoker, 1981; Lazutin et al., 2001]. Its intensification led to the fact that *substorm-1*

propagated to latitudes 77− 78° MLAT in the evening sector, and in the early evening sector it was observed even near the geomagnetic pole at 85° MLAT, at the THL observatory (magnetogram is not given here), where the polar part of the vortex propagates clockwise, as can be seen in the right AMPERE map 18:56− 19:06 UT in Fig. 2*a*.

Substorm-2, more intense than *substorm-1* (*AL* up to− 1500 nTL), with the activity maximum at ~21:30 UT was observed on the IMAGE profile in the near-midnight sector in the subauroral and auroral latitudes up to ~71° MLT without sharp bursts in the *Y* component of the magnetic field. Due to its location, IMAGE "sees" only one vortex located at latitudes 61− 67° MLAT from OUJ to SOR. The second vortex, whose center is located above 70° MLAT in the post-midnight sector, remains much further east.

Substorm-3, the most intense of the considered ones (*AL* less than− 1700 nTL) with the maximum activity at ~00:50 UT was observed on the IMAGE profile in the postmidnight-early-morning sector, since, according to the maps in Fig. *2c*, at this time the IMAGE meridian stations were located near the vortex center. Like *substorm-1*, it started at auroral latitudes (at ~57° MLAT, near NUR) and quickly reached polar latitudes. Its intensity at the maximum of the substorm at the stations (PEL-SOR) was noticeably higher than during *substorm-1*.

It is known [e.g., McPherron et al., 1973, 2016; Kerko et al., 2015] that a characteristic feature of a magnetospheric substorm is the formation of the substorm current wedge SCW (*Substorm Current Wedge*), which manifests itself as the development of positive magnetic bays at middle and low latitudes. The current wedge (SCW), appears as a 3-dimensional magnetosphere-ionosphere current system with currents flowing into the ionosphere in the morning and flowing out of it in the evening along the magnetic field lines and closing in the ionosphere by the western and eastern electrojets (detailed description is given, for example, in [Kerko et al., 2015; McPherron et al., 2016]. Inside the SCW region, the magnetic field component *X* is positive and symmetric about the central meridian of the current wedge. In turn, the *Y* component is asymmetric, positive to the west of the central meridian and negative to the east of it.

In the study of midlatitude magnetic observations during the discussed substorms, we used data from the IZMIRAN midlatitude stations located in the same longitude sector as the meridional profile of the IMAGE stations. To date, the IZMIRAN network equipped with the same-type magnetometers consists of 7 stations at latitudes from 34 to 60° MLAT. Data from magnetometers of 3 stations were used to analyze the selected substorms: MOS (Moscow, 51° MLAT, 111° MLONG), LPRS (Voronezh, 48° MLAT, 112° MLONG), SIM (Simeiz, Crimea, 40° MLAT, 115° MLONG), whose magnetograms are shown in Fig. 4. From Fig. 4*a* shows that each considered substorm was accompanied by positive variations in the *X*-component of the magnetic field at mid-latitudes, most

pronounced during *substorm-1*, which indicates the formation of the current wedge of the substorm. Positive variations of the *Y*-component of the magnetic field during these bays allow us to conclude that the center of the current wedge was located east of the IMAGE meridian. However, complex changes in the development of the geomagnetic situation during *substorm-3* were reflected in sharp jumps in the *Y*-component at the mid-latitude stations, from which one can conclude that the center of *substorm-3* moved rapidly along the latitude, since the meridian under consideration was located near the center of the powerful vortex.

Fig. 4.

6. DISCUSSION

Three intense substorms during the main phase of a strong magnetic storm are considered above. The first substorm developed at *SymH* around -50 nTL, the second around -80 nTL, and the third around -130 nTL, i.e., the amplitude of the substorms increased with increasing intensity of the magnetic storm, as can be seen in Fig. 1. The first of the considered substorms can be referred to the "isolated" substorms, because before it, at least during 3 h, there were no significant geomagnetic perturbations. The subsequent substorms began during the recovery phase of the previous substorms, and at the time preceding them (left AMPERE maps in Fig. 2), the western and eastern electrojet were registered at significantly lower latitudes than before the first substorm.

According to [Hoffman et al., 2010], the main difference between "storm" substorms and "isolated" substorms is that "storm" substorms are not accompanied by the development of WTS A typical indicator of WTS is the appearance of positive bursts in the *Y*-component of the geomagnetic field at the leading edge of the bulge [Kisabeth and Rostoker, 1973; Tighe and Rostoker, 1981]. In Fig. 3, where the magnetograms of some stations of the IMAGE profile are presented, we can see that positive bursts in the *Y*-component of the magnetic field at high latitudes were observed only during the *onset* of the first substorm, hence, it developed as an "isolated" substorm in contrast to the other substorms.

Analyzing the AMPERE maps, we found that the *onset* of all three substorms (middle plots in Fig. 2) was associated with the appearance of the ionospheric current vortex directed clockwise, which is an indicator of local strengthening of the incoming longitudinal currents, this is confirmed by the color maps of the distribution of longitudinal currents at the AMPERE site (not given in this paper). During the first and second substorms, such eddies during the onset of substorms at the IMAGE meridian (left maps in Fig. 2) were registered in the near-midnight sector

The morning vortices observed at the activity maxima (by *AL*-index) of all three substorms considered (right AMPERE maps in Fig. 2) were accompanied by much weaker vortices with the opposite direction of rotation of the vectors observed in the late afternoon sector (at about 15-18 MLT). A similar morning intensification of large-scale ionospheric currents near the activity maxima

of very intense substorms was also detected by the authors of [Ohtani et al., 2018] during four strong magnetic storms (October 22, 2001, November 20, 2003, December 14-15, 2006, and March 17−18, 2015. During the latter event, AMPERE project registration data were already available.

Let us compare our results with the global distribution of ionospheric currents from AMPERE maps (Fig. 5) during a superstorm (*AL*-index near− 2500 nTL) observed near the activity maximum of the main phase of a strong magnetic storm on March 17, 2015, discussed in the above paper [Ohtani et al., 2018]. The term "superstorm" (*SSS*) was proposed in [Tsurutani et al., 2015] for substorms with intensities of 2500 nTL or more. Fig. 5 shows the distribution of equivalent ionospheric currents obtained from the AMPERE maps at the maximum of the substorm activity registered in the storm of March 17, 2015. It can be seen that the AMPERE maps in Fig. 5 are very similar to the distribution maps of ionospheric currents during the substorms we studied in the magnetic storm of March 23, 2023 (right maps in Fig. 2).

Fig. 5.

The morning intensification of the westerly electrojet and the appearance of a vortex with a clockwise rotation direction, i.e., the intensification of the in-flowing longitudinal current, can also be seen in the maximum of superstorm activity in other strong storms previously discussed in the literature, e.g., September 7, 2017 in Fig. 5 in [Despirac et al., 2020]; December 20, 2015 in Fig. 5*c* in [Despirak et al., 2022]; May 28, 2011 in Fig. 3 in [Despirak et al., 2022a]; April 5, 2010 in Fig. 4 in [Daspirak et al., 2022b] and in Fig. 2*b* in [Gromova et al., 2022].

Thus, the morning spatial peculiarities of intense substorms during strong magnetic storms, observed as the appearance of current vortices and strengthening of the westerly electric jet in the morning sector, can be considered typical for strong magnetic storms.

According to [Gjerloev and Hoffman, 2014], the formation and development of a large-scale current system in the morning sector during the activity maximum of an intense substorm can be schematically represented as the result of the development of the so-called *double wedge system* in the magnetosphere, the scheme of which is shown in Fig. 6. As a result of the superposition of longitudinal currents, at the eastern end of the current wedge (i.e., in the morning), the inflow longitudinal currents will prevail and at the western end - the outflow currents. In the near midnight sector, a mixed layered structure of longitudinal currents will be observed. A similar situation was observed at the beginning of substorm-2 (Fig. 2*b*, center map).

Fig. 6.

Possible reasons for the morning intensification of the westerly electrojet and the inflow longitudinal current at the maximum of the activity of substorms recorded during the main phase of very large magnetic storms have been discussed in detail in [Ohtani et al., 2018; Ohtani and Motoba, 2023]. The authors considered various causes, such as enhanced convection due to external sources,

intrusion of energetic electrons due to increasing solar wind pressure, and drift of electrons injected in the night sector to the morning side, but have not yet been able to identify the most likely one.

7. CONCLUSIONS

The planetary features of the spatial and temporal distribution of ionospheric electrodes at the *onset* and maximum of activity of three very intense substorms (with *AL* from -1200 nTL to -1700 nTL) in the main phase of the strong magnetic storm March 23−24, 2023, revealed on the basis of the analysis of planetary magnetic measurements from 66 simultaneous low-orbit (780 km) satellites of the AMPERE project, have been considered.

It was found that the *onset* of all substorms at the IMAGE meridian was associated with the formation of a current vortex in auroral latitudes with a clockwise rotation direction, which is an indicator of local intensification of the inflow longitudinal currents. The analysis of mid-latitudinal observations at the stations of the IZMIRAN network showed that the center of the current wedge of the substorm at this time was located much to the east of the IMAGE meridian.

In the first, essentially isolated substorm to the west of the vortex, i.e. in the evening sector, one noted a rapid expansion of the western electric jet towards the pole and the development at its western edge of the WTS, manifested in ground-based geomagnetic observations at high-latitudinal stations of the IMAGE profile as a short positive burst in the *Y*-component of the field.

During the maximum of activity of the analyzed substorms, the development in the morning sector (05− 08 MLT) of a large-scale intense current vortex with a clockwise rotation direction was detected, indicating the intensification of the inflow longitudinal currents. The revealed effect was confirmed by analyzing the spatial features of the ionospheric current at the activity maximum of several superstorms discussed in the literature, observed in the main phase of strong magnetic storms. A similar morning enhancement of the inflow longitudinal currents during substorms in the main phase of four strong magnetic storms was also reported in [Ohtani et al., 2018]. Thus, the morning spatial features of very intense substorms during strong magnetic storms, such as the formation of current eddies with clockwise rotation direction (intensification of the inward flowing longitudinal currents) and the strengthening of the westerly electrojet in the morning sector and the easterly electrojet in the evening sector, that we have identified, can be considered typical of very intense substorms.

ACKNOWLEDGMENTS

The authors thank the creators of the IMAGE meridional network (https://space.fmi.fi/image/) and IZMIRAN magnetometer network (http://serv.izmiran.ru) databases, as well as the AMPERE project (http://ampere.jhuapl.edu/products) for the possibility to use the data in the ongoing studies.

FUNDING

The research was carried out within the framework of the State Assignments of the institutes.

REFERENCES

1. *Despirak I.V., Kleymenova N.G., Gromova L.I., Gromov S.V., Malysheva L.M.* Supersubstorms during the storms of September 7–8, 2017 // Geomagnetism and Aeronomy. V. 60. No. 3. P. 308–317. 2020. https://doi.org/10.31857/S0016794020030049

2. *Despirak I.V., Kleymenova N.G., Lyubchich A.A., Setsko P.V., Gromova L.I., Werner R.* Global development of the supersubstorm on May 28, 2011 // Geomagnetism and Aeronomy. V. 62. No. 3. P. 325–335. 2022a. https://doi.org/10.1134/S0016793222030069

3. *Despirak I.V., Kleymenova N.G., Gromova L.I., Lyubchich A.A., Gineva V., Setsko P.V.* Spatial Features of the Supersubstorm during the Main Phase of the Storm on April 5, 2010 // Izv. RAS. Phys. Ser. V. 86. No. 3. P. 249-255. 2022b. https://doi.org/10.3103/S106287382203008X

4. *Ishkov V.N.* Results and Lessons of Cycle 24 – the First Cycle of the Second Epoch of Reduced Solar Activity // Astron. J. V. 99. No. 1. P. 2022. https://doi.org/10.31857/S0004629922020050

5. *Ishkov V.N.* Current 25th cycle of solar activity on the eve of the maximum phase // Proceedings of the XXVII All-Russian annual conference on solar physics "Solar and solar-terrestrial physics - 2023". St. Petersburg. P. 139-144. 2023. https://doi.org/10.31725/0552-5829-2023-139-144

6. *Kornilova T.A., Kornilov I.A.* Spatio-temporal dynamics of auroras during the main phase of a magnetic storm // Geomagnetism and aeronomy. V. 49. No. 6. P. 757-767. 2009.

7. *Akasofu S.-I, Chapman S.* The development of the main phase of magnetic storms //J. Geophys. Res. V. 68. P. 125–129. 1963. https://doi.org/10.1029/jz068i001p00125

8. *Boudouridis A., Zesta E., Lyons L.R., Anderson P.C., Lummerzheim D.* Effect of solar wind pressure pulses on the size and strength of the auroral oval // J. Geophys. Res. 2003. V. 108. N A4. P. 8012 – 8027. https://doi.org/10.1029/2002JA009373

9. *Baumjohann W., Kamide Y., Nakamura R.* Substorms, storms and the near-Earth tail //J. Geomagn. Geoelectr. V. 48. I. 2. P. 177−185. 1996. https://doi.org/10.5636/jgg.48.177

10. *Despirak I.V., Lubchich A.A., Kleimenova N.G., Setsko P.V., Werner R.* Supersubstorm on 20 December 2015: Spatial Geomagnetic Effects // Proceedings of the Fourteenth Workshop “Solar Influences on the Magnetosphere, Ionosphere and Atmosphere”. P. 10−15. 2022. https://doi.org/DOI: 10.31401/WS.2022.proc

11. *Ebihara Y., Tanaka T.* Substorm simulation: Formation of westward traveling surge // J. Geophys. Res. Space Physics. V. 120. P.10466–10484. 2015. https://doi/org/10.1002/2015JA021697.

12. *Feldstein Y.I., Grafe A., Gromova I.I., Popov V.A.* Auroral electrojets during geomagnetic storms // J. Geophys. Res. V. 102. P. 14223–14235. 1997. https://doi:10.1029/97JA00577

13. *Gjerloev J.W., Hoffman R. A., Sigwarth J. B., Frank L. A., Baker J. B.* Typical auroral substorm: A bifurcated oval. // J. Geophys. Res. V. 113. A03211. 2008. https://doi:10.1029/2007JA012431

14. *Gjerloev J.W., Hoffman R.A.* The large-scale current system during auroral substorms. // J. Geophys. Res.: Space Physics. V. 119. P. 4591–4606. 2014. https://doi.org/10.1002/2013JA019176

15. *Gromova L.I., Kleimenova N.G., Despirak I.V., Gromov S.V., Lubchich A.A., Malysheva L.M.* Magnetic storm 20 April 2020: substorms in the main phase // 'Physics of auroral phenomena', Proceedings of the 45th Annual Seminar. P .16−19. 2022. https://doi.org/10.51981/2588-0039.2022.45

16. *Hoffman R.A., Gjerloev J.W., Frank L.A., Sigwarth, J.W.* Are there optical differences between storm-time substorms and isolated substorms? //Ann. Geophys. V. 28. P. 1183–1198. 2010. https://doi.org/10.5194/angeo-28-1183-2010

17. *Hsu T.-S., McPherron R.L.* The Characteristics of Storm-Time Substorms and Non-Storm Substorms // Fifth International Conference on Substorms. Edited by A. Wilson. ESA SP-443. P. 439−442. 2000.

18. *Kamide Y., Ahn B.-H., Akasofu S.-I., et al.* Global distribution of ionospheric and field-aligned currents during substorms as determined from six IMS meridian chains of magnetometers: initial results //J. Geophys. Res. V. 87. P. 8228–8240. 1982. https://doi.org/10.1029/JA087iA10p08228

19. *Kepko L., McPherron R.L., Amm O., Apatenkov S., Baumjohann W., Birn J., Lester M., Nakamura R., Pulkkinen T.I., Sergeev V.* Substorm current wedge revisited. // Space Sci. Rev. V. 190(1-4). P. 1–46. 2015. https://doi.org/10.1007/s11214-014-0124-9

20. *Kisabeth J., Rostoker G.* Current flow in auroral loops and surges inferred from ground-based magnetic observations. //J. Geophys. Res. V. 78. P. 5573–5584. 1973. https://doi.org/10.1029/JA078i025p05573

21. *Lazutin L., Starkov G., Meng C-I., Sibeck D.G., Stadsnes J., Bjordal J., Kan Liou, Kornilova T., Reeves G.* Westward traveling surge dynamics and the local structure of an isolated substorm. // Adv. Space Res. V. 28. P. 1623−1629. 2001. https://doi.org/10.1016/S0273-1177(01)00489-6

22. *McPherron R.L., Russell C.T., Aubry M.P.* Satellite studies of magnetospheric substorms on August 15, 1968: 9. Phenomenological model for substorms // J. Geophys. Res. V. 78. N 16. P. 3131−3149. 1973. https://doi.org/10.1029/JA078i016p03131

23. *McPherron R.L., Chu X.* Relation of the auroral substorm to the substorm current wedge. //G*eosci. Lett.* V. 3. P. 12. 2016. https://doi.org/10.1186/s40562-016-0044-5

24. *Ohtani S., Motoba T., Gkioulidou M., Takahashi K., Singer H. J.* Spatial development of the dipolarization region in the inner magnetosphere. //J. Geophys. Res.: Space Physics. V. 123. P. 5452–5463. 2018. https://doi.org/10.1029/2018JA025443

25. *Ohtani S., Motoba T.* Formation of beading auroral arcs at substorm onset: implications of its variability into the generation process. //J. Geophys. Res.: Space Physics. V. 128. e2022JA030796. 2023. https://doi.org/10.1029/2022JA030796

26. *Tighe W.G. and Rostoker G.* Characteristics of westward travelling surges during magnetospheric substorms. //Journal of Geophysics - Zeitschrift fuer Geophysik. V. 50. N 1. P. 51−67. 1981.
27. *Troshichev O.A., Podorozhkina N.A., Sormakov D.A., Janzhura A.S.* PC index as a proxy of the solar wind energy that entered into the magnetosphere: Development of magnetic substorms // J. Geophys. Res.:Space Physics. V. 119. P. 6521–6540. 2014. https://doi.org/10.1002/2014JA019940
28. *Tsurutani B.T., Hajra R., Echer E., Gjerloev, J.W.* Extremely intense (SML ≤ -2500 nT) substorms: isolated events that are externally triggered? // Ann. Geophys. V. 33. P. 519–524. 2015 https://doi.org/10.5194/angeocom-33-519-2015

FIGURE CAPTIONS

Fig. 1. Variations of the geomagnetic activity indices (*SymH, AL, PC*), MMP components (*B, By, Bz*) and solar wind parameters (velocity *V* and dynamic pressure *Psw*). Arrows are the considered substorms. The horizontal line is the analyzed interval.

Fig. 2. AMPERE maps of the electrojet positions during *substorms 1, 2* and *3 (a,b,c, respectively)*: left maps− before the beginning of the substorm, central− at the moment of its beginning and right− near the activity maximum. Arrows− position of the IMAGE meridian.

Fig.3. Magnetograms: (*a*) *X*- and (*b*) *Y*-components of the field of some stations of the IMAGE chain. The thick arrows schematically show the activity maxima of the considered substorms.

Fig. 4. Magnetograms: (*a*) *X*- and (*b*) *Y*-components of the midlatitude stations of IZMIRAN.

Fig. 5. The March 17, 2015 event: AMPERE map of the electrojet positions near the maximum of substorm activity. The arrows are the IMAGE meridian position.

Fig. 6. Schematic of the large-scale substorm current system: morning double current wedge of the substorm, from [Gjerloev and Hoffman, 2014].

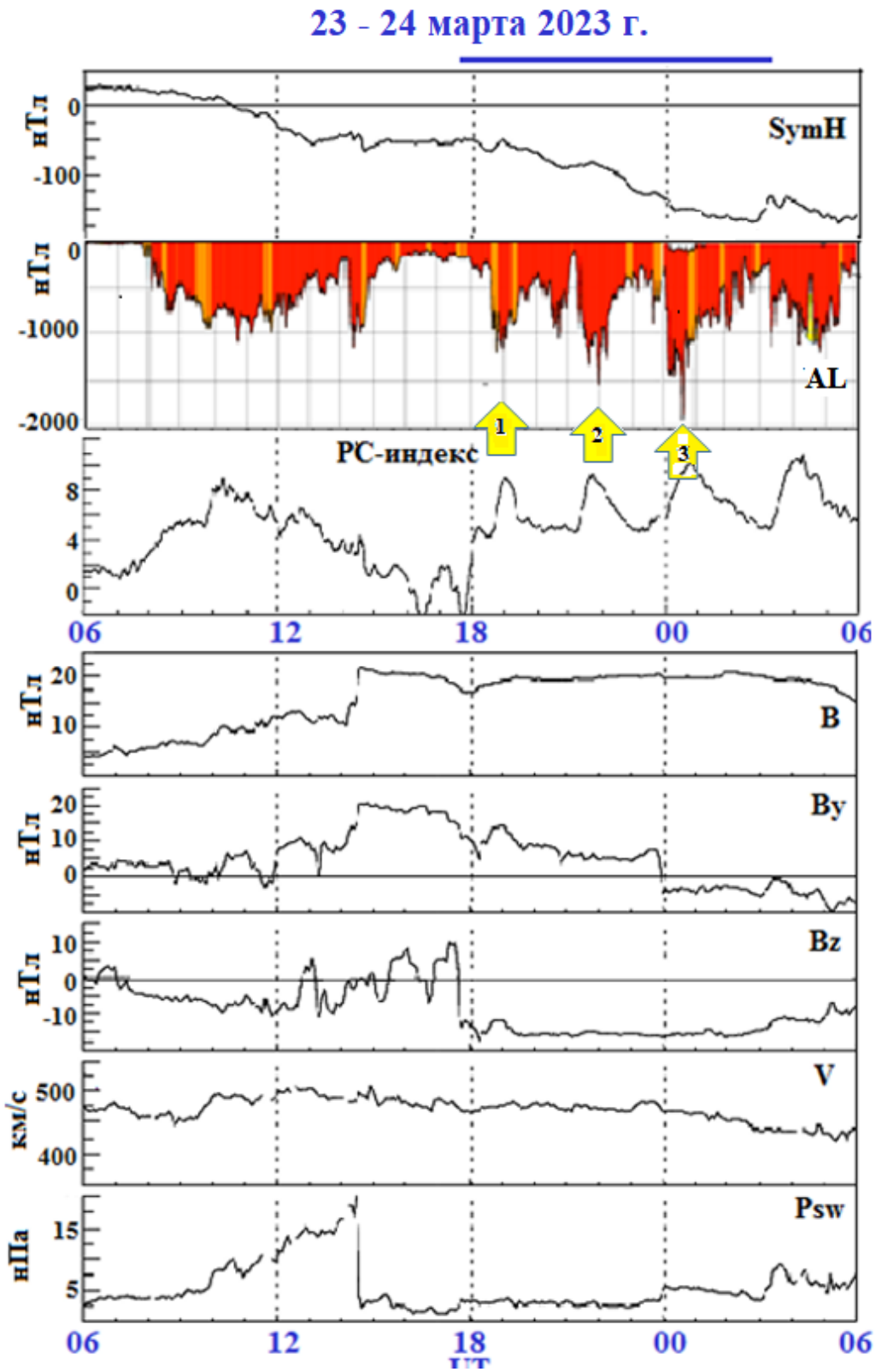
23 - 24 марта 2023 г.
нТл
0
-100
SymH
нТл
0
-1000
-2000
AL
1
2
3
РС-индекс
8
4
0
06
12
18
00
06
нТл
20
10
B
нТл
20
10
0
By
нТл
10
0
-10
Bz
км/с
500
400
V
нПа
15
5
Psw
06
12
18
00
06
UT

Fig. 1.

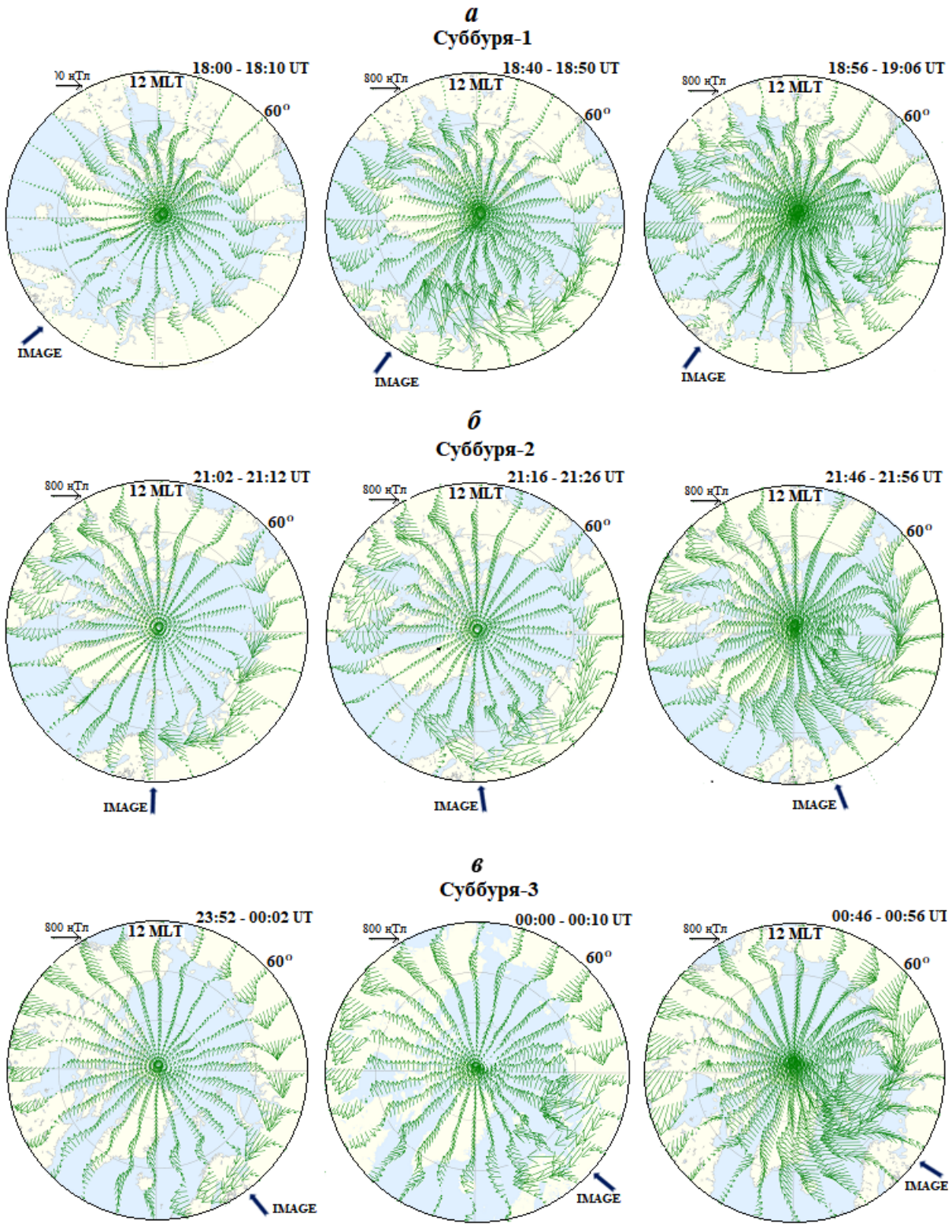
а
Суббуря-1
18:00 - 18:10 UT
18:40 - 18:50 UT
18:56 - 19:06 UT
12 MLT
60°
IMAGE
б
Суббуря-2
21:02 - 21:12 UT
21:16 - 21:26 UT
21:46 - 21:56 UT
в
Суббуря-3
23:52 - 00:02 UT
00:00 - 00:10 UT
00:46 - 00:56 UT

Fig. 2.

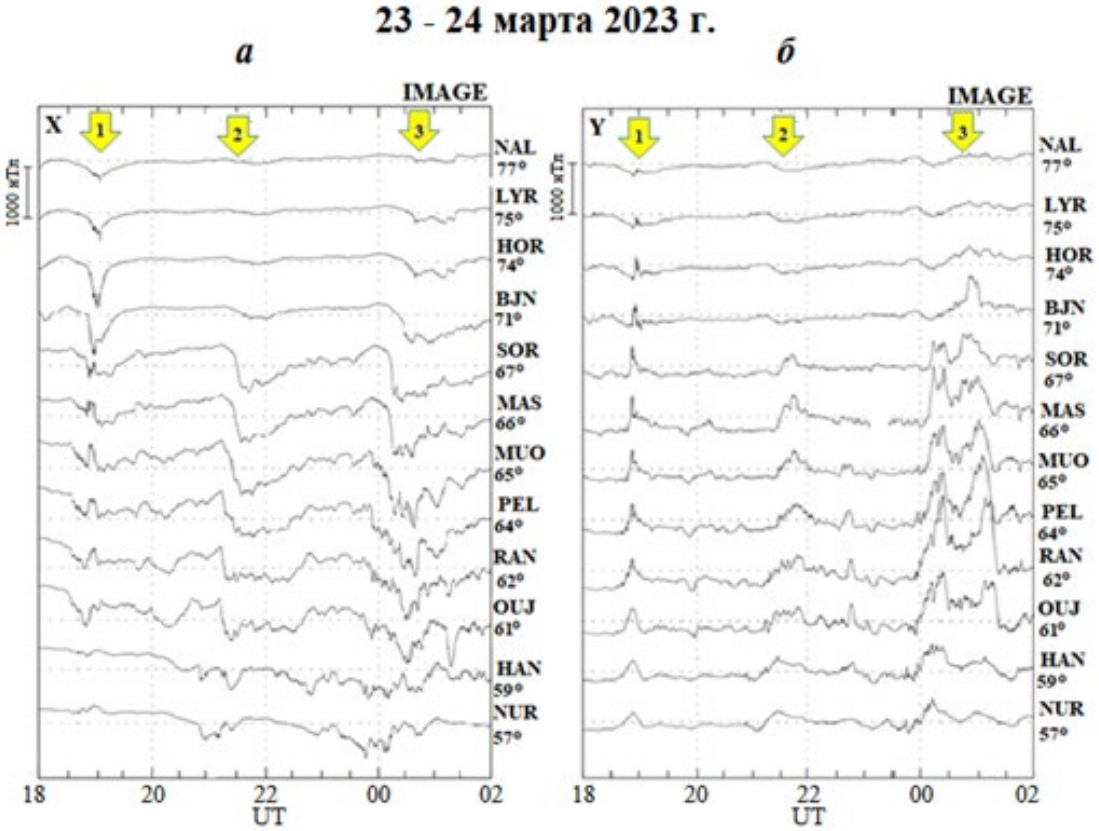
23 - 24 марта 2023 г.
а
б
IMAGE
X
Y
1
2
3
1000 нТл
NAL 77°
LYR 75°
HOR 74°
BJN 71°
SOR 67°
MAS 66°
MUO 65°
PEL 64°
RAN 62°
OUJ 61°
HAN 59°
NUR 57°
18
20
22
00
02
UT

Fig. 3.

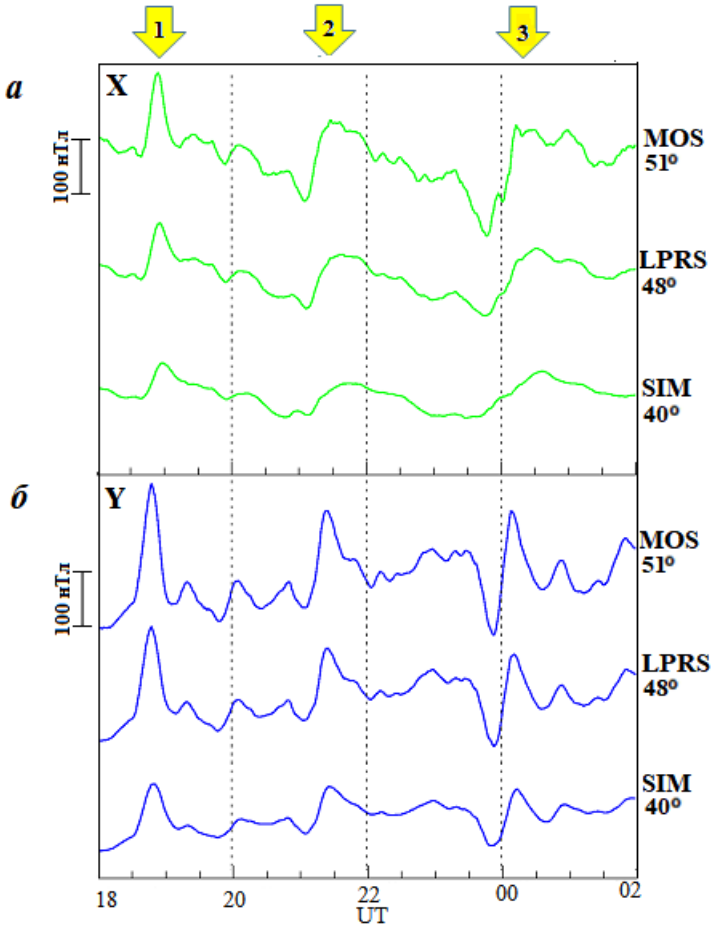
1
2
3
а
X
100 нТл
MOS
51°
LPRS
48°
SIM
40°
б
Y
100 нТл
MOS
51°
LPRS
48°
SIM
40°
18
20
22
00
02
UT

Fig. 4.

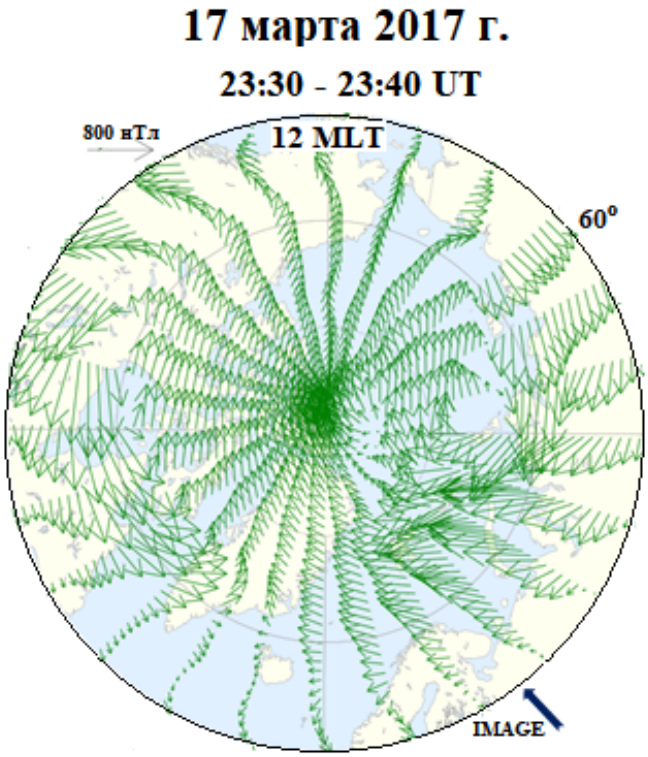

Fig. 5.

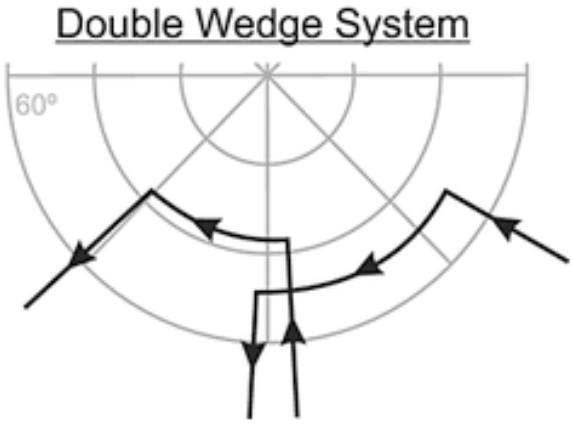

Fig. 6.